Journal of Advanced Ceramics
2018, **7**(1): 5–16
https://doi.org/10.1007/s40145-017-0251-3

ISSN 2226-4108
CN 10-1154/TQ

Research Article

Effects of regenerative mechanical vibration on the mechanical integrity of ceramic diesel particulate filters

Gbadebo OWOLABI[a,*], Akindele ODESHI[a,b], Paul RAGALLER[c], Alexander SAPPOK[c]

[a]*Department of Mechanical Engineering, Howard University, Washington, DC, USA*
[b]*Department of Mechanical Engineering, University of Saskatchewan, Saskatoon, Canada*
[c]*CTS Corporation Boston Innovation Office, Malden, MA, USA*

Received: June 11, 2017; Revised: September 28, 2017; Accepted: October 16, 2017

Abstract: In this study, the effects of mechanical vibration on the mechanical properties of ceramic diesel particulate filters (DPFs) were investigated. The goal is to determine how the mechanical vibration used in the regenerative ash cleaning process for these filters affects their mechanical integrity during subsequent reuse. Both virgin and vibrated DPF samples were subjected to compressive and 3-point flexural loading at three different loading rates along axial and tangential directions. Statistical analysis was conducted to determine the significance of variation in the compressive and flexural strengths of the DPFs as a result of exposure to mechanical vibration. The results show that there is no statistically significant difference in both compressive and flexural strengths of the virgin DPFs and the DPFs subjected to the same level of mechanical vibration typically used in ash cleaning of DPFs. When the intensity of vibration was doubled, the drop in compressive strength became statistically significant, but less than 10% under axial loading. However, no drop in flexural strength was observed for DPFs subjected to this high intensity of mechanical vibration. The safe threshold for mechanical vibration of ceramic filters is considered to be much higher than that currently used in vibration-based ash cleaning process.

Keywords: diesel particulate filter (DPF); cordierite; mechanical testing; filter regeneration; vibration-based ash cleaning technology

1 Introduction

Fuel combustion in heavy duty diesel trucks, with no emission control system or retrofits, releases harmful particulate matter (PM) or soot into the atmosphere. Constituents of the diesel particulate matter can include carbon, inorganic oxides, and highly toxic hydrocarbons [1]. When inhaled, PM can penetrate into the lung, carrying toxic substances that can trigger respiratory and cardiovascular disease. Johnson and Parker [2] provided an overview of the epidemiological studies showing a strong correlation between cardiovascular diseases and air pollution. A World Health Organisation's report suggested that 3% of cardiopulmonary and 5% of lung cancer diseases can be traced to the adverse effects of inhaled PM [3]. The toxicity of the airborne particles is reported to increase with decrease in particle size [4]. Seaton *et al.* [5] reported that although relatively large

* Corresponding author.
E-mail: gbadebo.owolabi@howard.edu

airborne particles can be removed by settling in a matter of hours, fine particles can be suspended in the atmosphere for weeks. Thus, fine particles can easily accumulate causing incalculable damage to the quality of life in urban centres. In order to decrease mortality and morbidity associated with high concentration of PM in the atmosphere, emission of PM needs to be strictly controlled.

One of the major sources of PM in the atmosphere is fuel combustion in the engines of heavy duty diesel engine vehicles. PM emission in combustion engines can be reduced by raising combustion temperature, but a higher combustion temperature will increase NO_x emission [1]. It is estimated that about 50% of NO_x gases in the atmosphere are emitted from combustion of automobiles and diesel engine trucks while 20% come from electric power plants [6]. NO_x reacts with volatile organic compounds in the atmosphere in the presence of sunlight to form ozone [7], exposure to which can also result in considerable health burden [8]. Reduction in NO_x emission can be achieved by better combustion control through efficient nozzle design [9], exhaust gas recirculation [10], selective catalytic reduction of NO_x [11,12], among others. Some of these measures can however cause increase in PM emission. There must therefore be a trade-off between PM and NO_x emission in diesel engines. Diesel particulate filters (DPFs) are developed to remove PM from the exhaust gases of heavy duty diesel engine trucks [13–15]. They are essentially porous or honeycomb-type materials through which exhaust gas flow and in which PM can be trapped. Some of the base materials used in making porous ceramic filters include silicon carbide, silicon nitride, mullite, aluminum titanate, and cordierite [1]. Porous thermal resistant metallic materials consisting of sintered metal fibers have also been developed for use as DPF to remove PM from diesel power generators [16]. Honeycomb-type ceramic materials are commonly used as DPF for heavy duty diesel engine vehicles.

Ceramic DPFs such as honeycomb structured cordierite have been coated with NO_x reduction catalysts to provide a filtering system that can simultaneously remove both PM and NO_x from diesel engines [17]. Growing nanofibers of SiC on the inner walls of the channels of the cordierite DPF is reported to offer an advantage of increasing the filtration efficiency for submicron PM and providing surface area support for noble metal catalysts in the channels [18]. An underlining challenge associated with the use of DPFs is the eventual clogging of the filter with soot or ashes after prolonged use. This will lead to increase in backpressure and increase in fuel consumption [19]. Sooth deposition on the wall of the DPF was investigated by Bensaid *et al.* [20], who observed a correlation between the pressure drop and filtration efficiency. Combustion to burn off accumulated PM on the walls of DPF is often used to regenerate clogged DPF. This can be done by raising the temperature of the exhaust gas [1]. Thermal combustion of sooth is not without its own challenges as thermal stresses can develop leading to DPF cracking [21]. In addition, incombustible ash residue generated from combustion of PM and other combustible materials in the exhaust gases can accumulate over a period of time and eventually clog the DPF.

AccelaClean^{TM} vibration-based cleaning technology developed by Filter Sensing Technology (FST) Inc. has been found to be very effective for ash removal from ceramic DPF. In this process, mechanical vibration is used to break up the ash plug and remove them from the channels of the cordierite DPF during the ash cleaning process. As a result of its good resistance to thermal shock, cordierite is one of the most popular materials used in making ceramic DPF. Porous cordierite contains micro-cracks [22], which mostly develop during thermal processing. The level of porosity and the presence of these micro-cracks will influence the mechanical properties of cordierite. Gordon *et al.* [23] reported the fracture toughness of monolithic cordierite to be about 0.242 $MPa \cdot m^{1/2}$, while the cordierite investigated by Shyam *et al.* [24] was determined to have fracture toughness that varies between 0.38 and 0.45 $MPa \cdot m^{1/2}$, depending on notch orientation. Fracture toughness of cordierite has been reported to decrease with increase in porosity [23]. Depending on the sintering temperature, Suzuki *et al.* [25] determined the fracture toughness of dense cordierite to range between 2 and 3 $MPa \cdot m^{1/2}$. The Young's modulus of cordierite has been reported to increase from 11.9 GPa at 23 ℃ to 16.3 GPa at 1000 ℃ while the Poisson ration remained nearly the same in this temperature range [24]. The increase in strength with increase in temperature was attributed to self-healing of the micro-cracks at high temperatures. This attribute is very significant for high temperature application of cordierite in DPF. Pandey *et al.* [26] reported nonlinear stress–strain relation during tensile testing of the thin wall of cordierite-based PDF and reported a correlation between the nonlinearity of tensile response to the initial density of micro-cracks in the material.

Besides thermal-induced cracking, there have been reported cases of melting of cordierite DPF during

injection of fuel to heat up and regenerate the filter [27]. Despite this shortcoming, cordierite remains one of the most popular ceramic materials used in DPF. Vibration-based cleaning for ash removal remains a very viable option for regeneration of cordierite DPF. It is however not clear how the mechanical vibration used in ash removal will affect the mechanical properties of the regenerated cordierite DPF and its performance during subsequent use. This is the focus of the current investigations. Most of the previous investigations on mechanical behaviour of cordierite were conducted on the thin wall of DPF. In the current study, mechanical behaviour of the honeycomb structure as affected by vibration-induced cleaning is reported.

2 Materials and methods

Honeycomb-type cordierite DPF (Fig. 1) produced by Corning Inc. was used in this study. Three different categories of the cordierite-based DPF were supplied by FST Inc. for this investigation. The first category was not subjected to mechanical vibration and it is code-named DPF-Virgin in this paper. The second category was subjected to mechanical vibration using maximum absolute acceleration of 221*g*, which is the intensity of vibration typically used by FST for ash removal during DPF regeneration process [28]. This code-named DPF-NmViB with "Nm" standing for the normal level of applied vibration. The last sample was exposed to vibration at maximum acceleration of 506*g*, which is more than twice the intensity of vibration used in ash cleaning process. This is code-named DPF-ExViB with "Ex" standing for vibration level in excess of that used for ash cleaning. The samples were subjected to 9 consecutive 10-min vibration cycles.

The cylindrical DPF samples (as-received and vibrated) were dry-cut into rectangular test specimens for mechanical testing. The dimensions of the test specimens are presented in Fig. 2. Uniaxial compressive test and 3-point bending test were conducted on the specimens at crosshead speeds of 0.5, 1.0, and 1.5 mm/min. Instron 5500 universal testing machine with 100 kN load cell was used for the compression test while the bending test was conducted using Instron 3368 universal testing machine with a 1 kN load cell. Tissue papers were placed between the pliable ceramic DPF specimens and the hard loading steel frame to smoothen and soften the contact, thereby preventing premature failure of the DPF due to surface roughness. The specimens were tested under axial and tangential loads to determine the effects of loading direction on the strength of the DPFs as shown in Fig. 2. Cold-crush test according to the ASTM C133 standard was used for the determination of the compressive strength. The 3-point bending test was conducted according to the ASTM C1674 standard using a span of 90 mm.

The specimens for optical and scanning electron microscopic investigations were prepared by cold-mounting using acrylic resin, followed by grinding using 500, 1200, 2000, and 4000 FEPAP grade SiC paper in that order. Optical microscopic investigation was done using Nikon Eclipse MA 200 optical microscope coupled with NIS Element D image analysis system. The specimens for scanning electron microscopy (SEM) and energy dispersive X-ray spectroscopy (EDS) analyses were coated with thin film of gold. The SEM images were acquired using JEOL JSM-6010LV scanning electron microscope using back scattered electron imaging at accelerated voltage of 15 kV. The energy dispersive X-ray (EDX) analysis was done using JEOL JSM-7600F field emission scanning electron microscope coupled with INCA EDS system produced by Oxford Instruments.

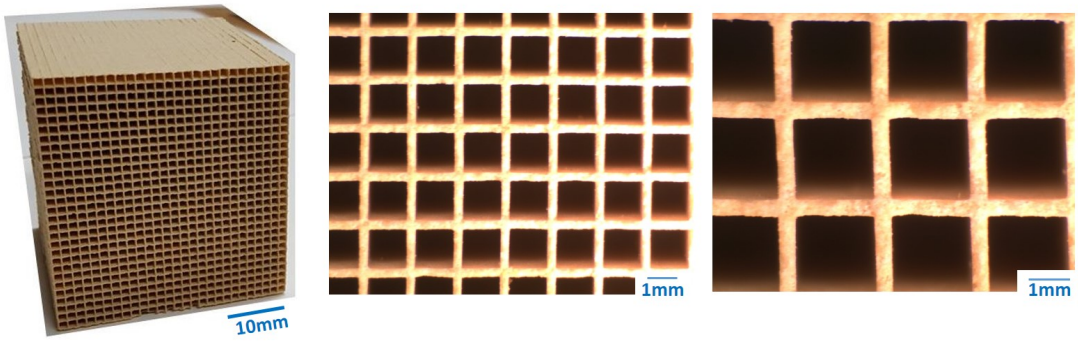

Fig. 1 Photographs of the investigated cordierite DPF showing the cellular structure.

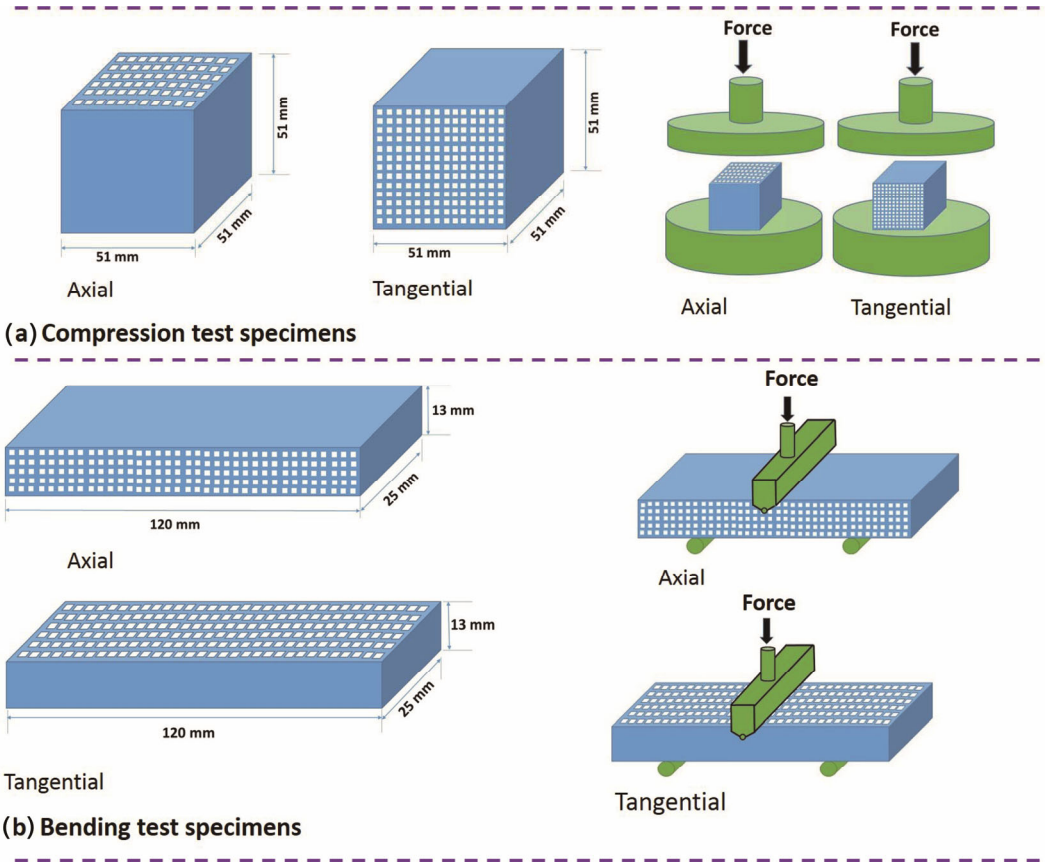

Fig. 2 Geometry of the test specimens: (a) compressive and (b) bending test specimens.

3 Experimental results

3. 1 Physical, microstructural, and compositional analyses of the investigated DPF

The density of the cordierite base materials used in producing the investigated DPF was determined using nitrogen gas operated pycnometer. For measurement using pycnometer, the mass of a piece of the cordierite wall was measured on weighing scale while its volume was determined using the pycnometer. The average density obtained from ten measurements is 2.31 ± 0.02 g/cm^3. The error in this value is the standard deviation. The density of a pure dense cordierite is reported to be 2.1 g/cm^3 [1]. Goren *et al.* [29] determined the density of synthetic cordierite powder made from talc, diatomite, and alumina to range between 2.24 and 2.47 g/cm^3 depending on the sintering temperature during processing. In another study, Njoya *et al.* [30] synthesized cordierite and determined its density to range between 2.2 and 2.6 g/cm^3 depending on the sintering temperature. The slight difference in densities reported for cordierite in the literature is due to differences in their processing conditions, especially the sintering temperature. The density recorded for the cordierite investigated in this study lies within the range reported in the literature.

Photographs of the DPF showing the cellular structure at different magnifications are presented in Fig. 1. Optical and scanning electron micrographs of a polished transverse section at higher magnifications are presented in Fig. 3. Using the analytical tools offered in the NIS D image analysis software, the average thickness of the walls of the DPF was determined to be 0.304 mm. The average size of each cell was determined to be about 1.45 mm × 1.45 mm. The results of the EDX analyses of the base filter material, as presented in Fig. 3(c), indicate that it consists mainly of oxygen, magnesium, aluminium, silicon, and traces of iron impurity. This confirms the continuous ceramic phase to be aluminium–magnesium–silicate ($Mg_2Al_4Si_5O_{18}$), i.e., cordierite. It is commonly produced from natural materials such as kaolin and talc [1]. The SEM micrographs of the cordierite wall of the DPF without mounting with polymer resin are presented in Fig. 4. They indicate the porosity of the filter material and the presence of micro-cracks. The widely dispersed pores are of varying sizes and irregular in shape. The micro-cracks

are suggested to develop in cordierite during high temperature processing [22]. The level of porosity and the presence of micro-cracks can have impact on the mechanical properties of a cordierite [23,24].

3. 2 Compression and flexural properties

Typical compressive and flexural stress–strain curves for both axial and tangential loading of DPF-NmViB specimens at crosshead speeds of 0.5, 1.0, and 1.5 mm/min are presented in Fig. 5. The trends of the stress–strain curves are similar for the three groups of DPFs (DPF-Vigin, DPF-NmViB, and DPF-ExViB) investigated in this study. The compressive stress–strain curves (Fig. 5(a)) show an initial nonlinearity after which the stress–strain relation becomes linear. The compressive stress eventually reaches a maximum value and then drops. The toe regions (non-linear) at the on-set of the stress–strain curves can be attributed to the crushing of slacks produced by protruded DPF walls and the seating of the specimens at the start of loading. Whereas the stress–strain curves of the samples loaded axially dropped only slightly beyond the maximum value and remained almost unchanged with further increase in strain, the stress of the specimens loaded tangentially dropped sharply as a result of catastrophic fracture of these specimens. The flexural stress–strain curves are characterised by discontinuities (Fig. 5(b)), which indicate the points at which cracking occurred in the wall of the DPF during loading. The stress increased linearly from the point of load application to fracture at the maximum load.

The average compressive and flexural strengths of

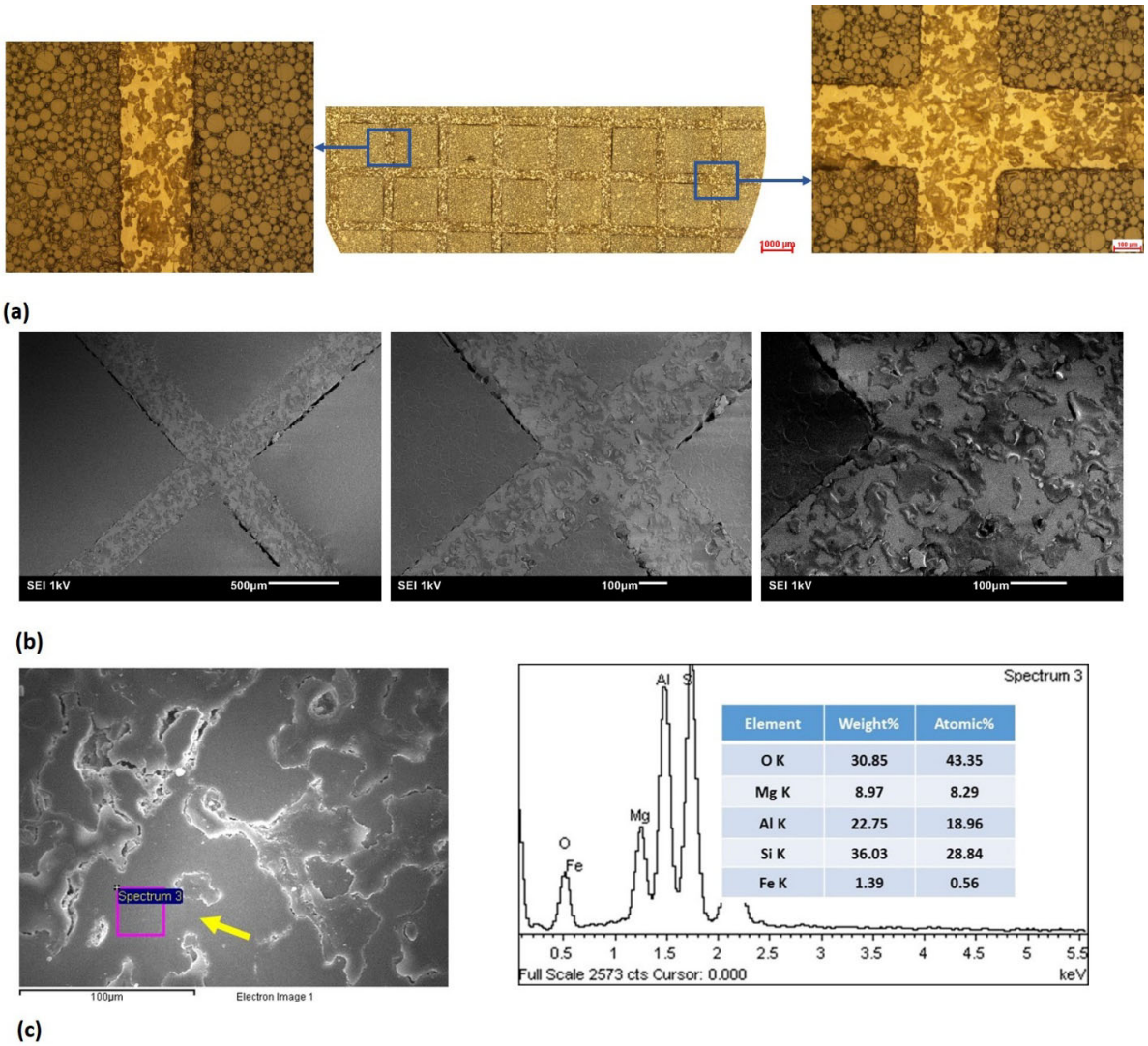

Fig. 3 (a) Optical and (b) SEM micrographs of the mounted and polished specimens of the cordierite-based DPF. (c) EDX analysis of the cordierite base material.

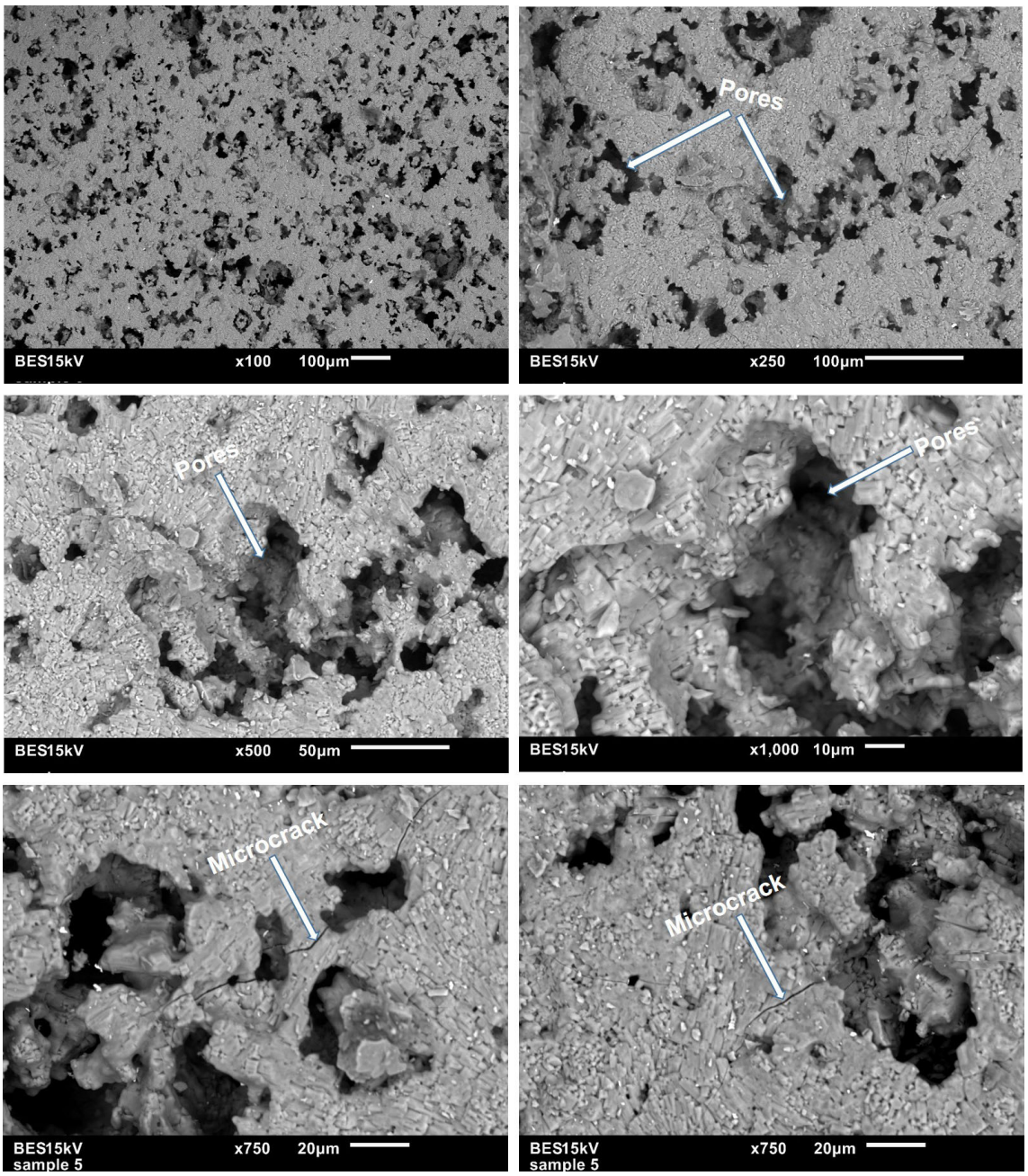

Fig. 4 SEM micrographs of the wall of the cordierite-based DPF at different magnifications showing porosity and presence of micro-cracks.

the specimens cut from the virgin DPF and the vibrated DPF are provided in Fig. 6. The average compressive strengths lie mostly between 4 and 5 MPa and between 1.5 and 2.0 MPa for specimens loaded axially and tangentially, respectively (Fig. 6(a)). These are averages for minimum of 5 test specimens subjected to the same test condition. These figures indicate no considerable influence of strain rates and mechanical vibration on the compressive strength of the cordierite DPF. Overall, no significant change was observed in the flexural strength as the crosshead speed was raised from 0.5 to 1.5 mm/min (Fig. 6(b)). The exception is in the case of specimens loaded in the axial direction, in which a decrease in flexural strength became significant as the crosshead speed was raised from 1.0 to 1.5 mm/min. It is evident from Fig. 6(b) that mechanical vibration at the levels investigated in this study (NmViB and ExViB) did not lead to any significant decrease in the modulus of rupture of the DPF when tested in both axial and tangential loading directions.

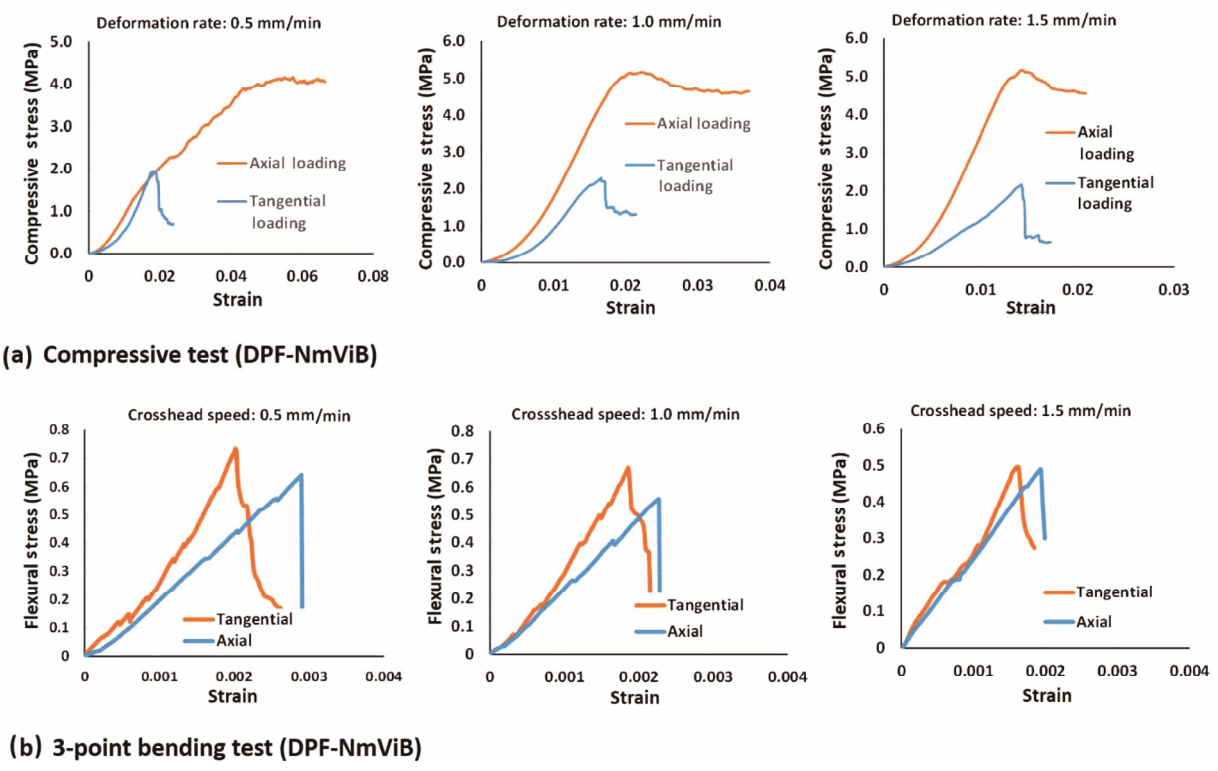

Fig. 5 Typical (a) compressive and (b) 3-point flexural stress–strain curves for DPF-NmViB (normal level of vibration).

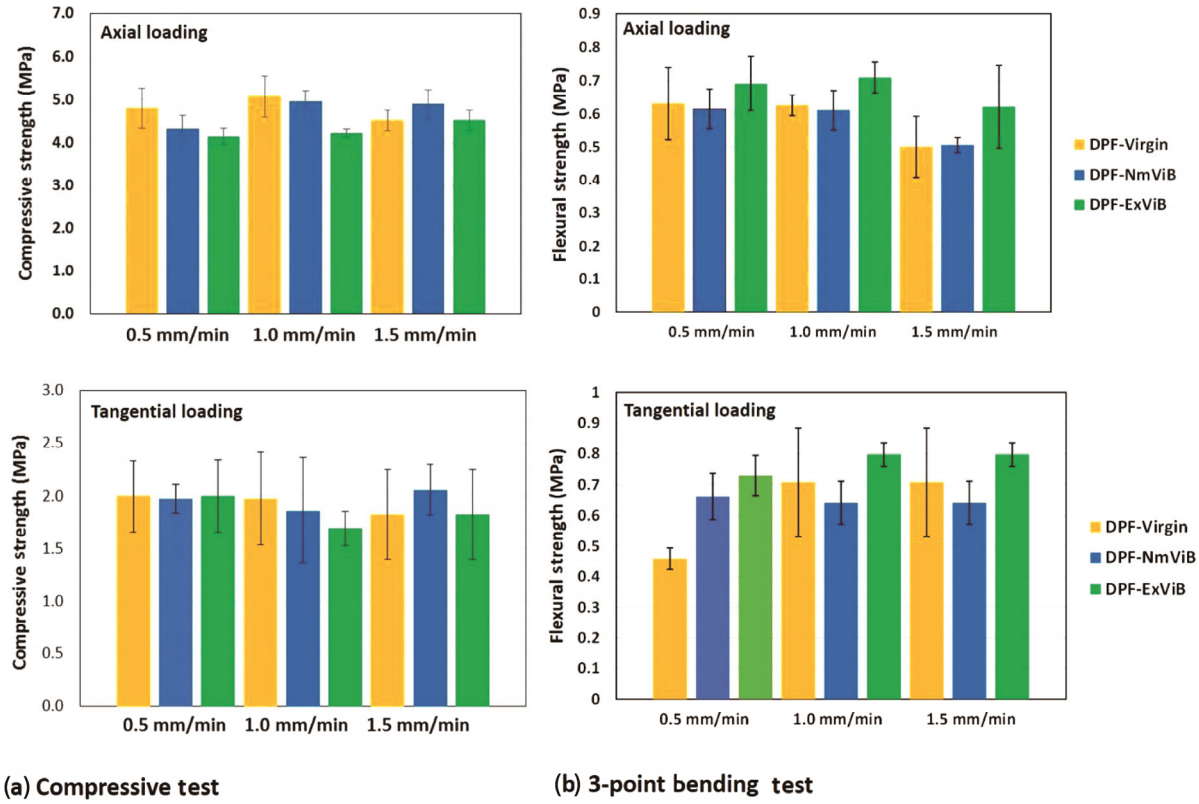

Fig. 6 (a) Compressive and (b) flexural strength of the investigated DPF as a function of deformation rate, loading direction, and applied mechanical vibration.

3. 3 Discussions

Optical images of some of the cordierite DPF specimens before and after mechanical testing in compression are presented in Fig. 7. Most of the DPF specimens (> 90%) loaded axially did not fracture at the maximum stress, but pulverized instead, at surfaces in contact with the bedding material during loading (Fig. 7(b)). The fine powder observed on the bedding material at the base of a test specimen subjected to axial loading is displayed in Fig. 7(b) (lower figure). A few axially loaded specimens cracked as shown in Fig. 7(c). Such cracking was observed mainly in specimens tested at the highest crosshead speed of 1.5 mm/min. On the other hand, all tangentially loaded specimens cracked and fractured (Fig. 7(d)). This led to the observed sharp drop in stress at maximum load in the stress–strain curves of the tangentially loaded specimens. We observed higher tendency for crack to develop and propagate in the DPF when the specimens were subjected to tangential compressive loading. This is unlike the case for the axially loaded DPF specimens, which rather pulverized at the loading surface instead of cracking under compressive loading. The higher cracking susceptibility of the DPF specimens when loaded tangentially accounts for the lower tangential compressive strength recorded in this study. This explains the significant difference in compressive strengths of the DPF under axial (4–5 MPa) and tangential (1.5–2.0 MPa) compressive loading.

Irrespective of the loading directions, the DPF specimens cracked or ruptured into two fragments under flexural loading (Fig. 8). This is responsible for the rapid drop in stress at maximum load as can be observed in Fig. 5(b). The failure of the DPF specimens under flexural loading was initiated at the point of maximum deflection on the outer surface of the test specimens (Fig. 8(b)) and propagated in the direction parallel to the loading plane towards the point of load application. From Fig. 6(b), it can be observed that the flexural strength of the DPF ranges between 0.48 and 0.72 MPa for axially loaded specimen and between 0.45 and 0.78 MPa for tangentially loaded specimens. The difference in axial and tangential strength under flexural loading is minimal compared to that under compressive loading, in which strength under axial loading is more than double that under tangential loading. The similar propensity of the DPF to crack when loaded either axially or tangentially under 3-point bending load accounts for the closeness of values of the flexural strength obtained for both loading directions.

The honeycomb-type cordierite-based ceramic DPFs were investigated in three states: (i) virgin state, i.e., no mechanical vibration (DPF-Virgin), (ii) normal vibration state, i.e., DPF subjected to mechanical vibration of the same intensity used in regenerative ash cleaning process (DPF-NmViB), and (iii) excessive vibration state, i.e., DPF subjected to mechanical vibration at intensity in excess of that used in vibrational ash cleaning process (DPF-ExViB). They were investigated at different deformation rates corresponding to crosshead speed of 0.5, 1.0, and 1.5 mm/min during mechanical testing,

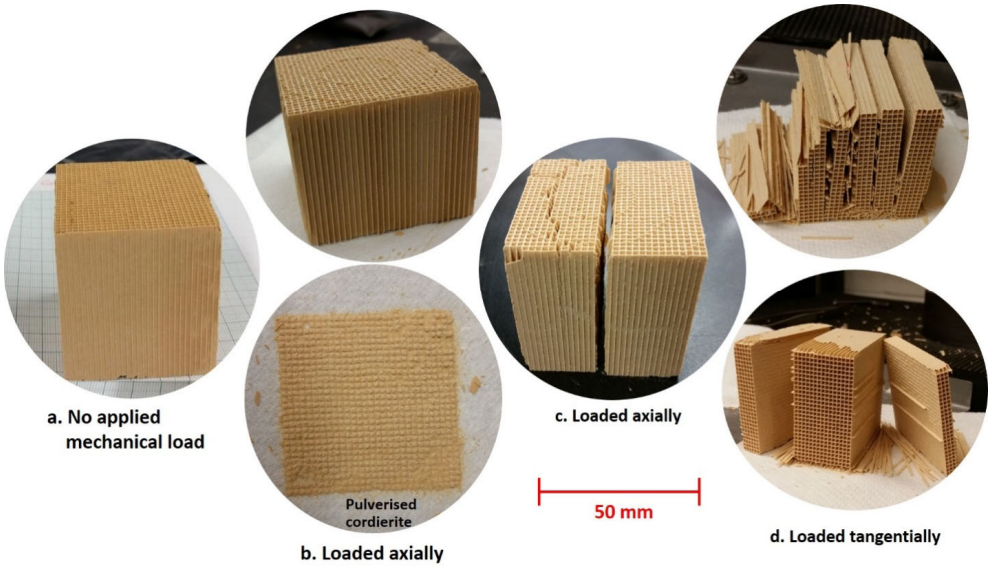

Fig. 7 Photographs of compressive test specimens: (a) before loading: no fracture; (b) after axial loading: no fracture; (c) after axial loading: fractured; and (d) tangentially loaded specimens: fractured.

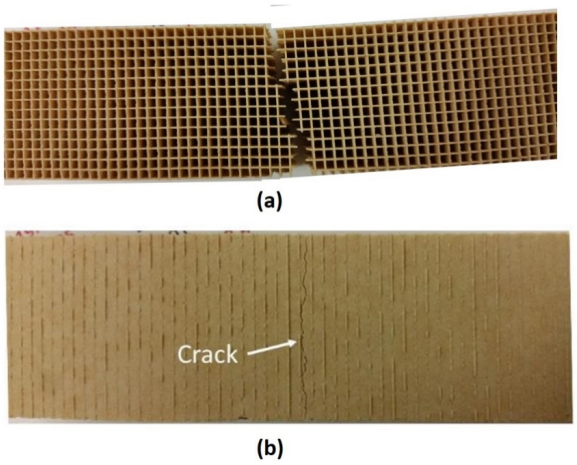

Fig. 8 (a) Fractured specimen after 3-point flexural loading and (b) crack at the point of maximum deflection in an axially loaded test specimen.

both in compression and in 3-point bending. The standard crosshead speed for testing this type of ceramic structure is about 1.0 mm/min. Mechanical loading of the DPF at crosshead speeds of 0.5 and 1.5 mm/min were included in this study to determine the effects of any change in crosshead speed, above or below the standard value of 1.0 mm/min, on the strength of the cordierite-based DPF. It can be observed from the scattering of the strength data that there is practically no significant difference in the compressive strength of the DPF specimens as the crosshead speed was raised from 0.5 to 1.5 mm/min (Fig. 6(a)). The recorded differences can be considered to be within the limit of experimental error. This is mostly true for both axial and tangential loading.

Since the influence of loading rates on compressive strength is insignificant, the average compressive strengths for all the investigated specimens irrespective of the crosshead speed were calculated and are presented in Fig. 9(a). Analysis of variance (ANOVA) was carry out to determine whether the difference between the compressive strengths of the virgin DPFs (DPF-Virgin), and those subjected to mechanical vibration (DPF-NmViB and DPF-ExViB) under axial and tangential loading are statistically significant. One factor ANOVA was done with the significant (or risk) level alpha (α) set at 0.05. The results, which are presented in Tables 1 and 2 indicate p-values that are less than 0.05, confirming statistically significant difference between the strengths of the 3 groups of DPFs. This is the case for both loading directions. However, when t-test was conducted to compare the strength of DPF-Virgin and the DPF-NmViB that was subjected to

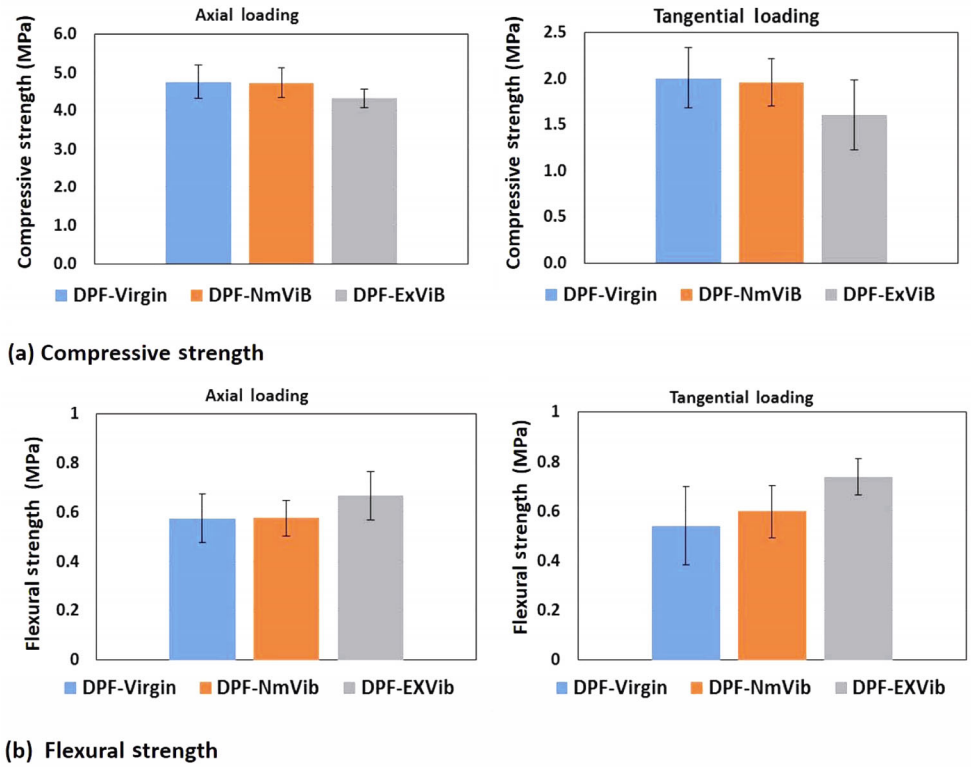

Fig. 9 Average (a) compressive and (b) flexural strength of all tested DPF specimens irrespective of the crosshead speed.

the normal level of mechanical vibration, the *p*-values were found to be higher than 0.05 (Tables 3 and 4). This suggests that the difference in the compressive strengths of DPF-Virgin and DPF-NmViB is not statistically significant. Increasing the intensity of vibration to about twice the normal intensity commercially used for ash cleaning lowered the compressive strength by 9% and 20% for specimens loaded axially and tangentially, respectively.

The average flexural strengths for all tested vibrated and virgin DPF specimens are compared in Fig. 9(b). There was no loss in flexural strength as a result of mechanical vibration of the DPF. The flexural strengths of the DPF specimens subjected to mechanical vibration were observed to be slightly higher than that for the specimens which were not exposed to mechanical vibration (DPF-Virgin). Although the reason for the slight increase in flexural strength is not quite clear, the results imply that mechanical vibration at both investigated intensities had no negative impact on the mechanical integrity of the DPF under 3-point bending load. Whereas micro-cracks originating from the voids in the DPF were observed in the DPF-Virgin as presented in Fig. 7, there is no evidence that the application of mechanical vibration resulted in the growth of these micro-cracks, which is in agreement with the results of the mechanical testing. Thus it can be concluded that the mechanical integrity of the DPF is not impaired by application of mechanical vibration with intensity of the same level used in AccelaClean^{TM} vibration-based ash cleaning technology for ceramic DPF. The result of two way t-test comparing the modulus of rupture when loaded axially and tangentially produced a *p*-value of 0.489 which is greater than set risk level 0.05. This confirms no statistically significant difference in flexural strength of the DPF when loaded in axial or tangential directions as indicated in Fig. 2.

Table 1 Result of one factor ANOVA test comparing the compressive strengths of DPF-Virgin, DPF-NmViB, and DPF-ExViB under axial loading

SUMMARY				
Group	Count	Sum	Average	Variance
DPF-Virgin	13	61.867	4.759	0.203
DPF-NmVib	13	61.675	4.744	0.160
DPF-ExViB	13	56.151	4.319	0.059

ANOVA						
Source of variation	SS	df	MS	F	*p*-value	F crit
Between groups	1.621	2	0.811	5.757	0.007	3.259
Within groups	5.069	36	0.141			
Total	6.690	38				

Table 2 Result of one factor ANOVA test comparing the compressive strengths of DPF-Virgin, DPF-NmViB, and DPF-ExViB under tangential loading

SUMMARY				
Group	Count	Sum	Average	Variance
DPF-Virgin	13	26.137	2.011	0.107
DPF-NmViB	14	27.497	1.964	0.105
DPF-ExViB	13	20.891	1.607	0.144

ANOVA						
Source of variation	SS	df	MS	F	*p*-value	F crit
Between groups	1.278	2	0.639	5.404	0.009	3.252
Within groups	4.375	37	0.118			
Total	5.653	39				

Table 3 Result of t-test comparing the axial compressive strengths of DPF-Virgin and DPF-NmViB under axial loading (assuming unequal variances)

	DPF-Virgin	DPF-NmViB
Mean	4.759	4.744
Variance	0.203	0.160
Observations	13	13
Hypothesized mean difference	0	
df	24	
t Stat	0.088	
P(T<=t) two-tail	0.930	
t Critical two-tail	2.064	

Table 4 Result of t-test comparing the compressive strengths of DPF-Virgin and DPF-NmViB under tangential loading (assuming unequal variances)

	DPF-Virgin	DPF-NmViB
Mean	2.011	1.964
Variance	0.107	0.105
Observations	13	14
Hypothesized mean difference	0	
df	25	
t Stat	0.371	
P(T<=t) two-tail	0.714	
t Critical two-tail	2.060	

4 Conclusions

The effects of mechanical vibration on the compressive

and flexural strengths of honeycomb-type ceramic diesel particulate filters were investigated. The purpose of this study is to determine whether the application of mechanical vibration used in regenerative ash cleaning of clogged DPFs will weaken the base material and impair the mechanical integrity of the filter. Research findings suggest no statistically significant difference in the compressive strength of DPF that was not subjected to mechanical vibration (DPF-Virgin) and that of the DPF that was subjected to the same vibration level that is normally used in ash cleaning of clogged filter (DPF-NmViB). This implies that the intensity of mechanical vibration currently used in ash cleaning of DPF is within the safe threshold for ash cleaning of clogged DPF and will not impair its mechanical integrity. However, increasing the intensity of vibration to about double the level used for ash cleaning decreased the compressive strength by 9% and 20% when loaded axially and tangentially, respectively. Interestingly, this did not lead to any noticeable decrease in flexural strength.

Acknowledgements

This material is based upon work supported by the National Science Foundation under Grant No. 1230444. The authors would like to thank Dr. Anthony Walters and Dr. Prakash Balan for their support and engaging discussions.

References

[1] Adler J. Ceramic diesel particulate filters. *Int J Appl Ceram Tec* 2005, **2**: 429–439.

[2] Johnson D, Parker JD. Air pollution exposure and self-reported cardiovascular disease. *Environ Res* 2009, **109**: 582–589.

[3] World Health Organization. Health effects of particulate matter. Policy implications for countries in eastern Europe, Caucasus and central Asia (2013). Available at http://www.euro.who.int/__data/assets/pdf_file/0006/189051/Health-effects-of-particulate-matter-final-Eng.pdf.

[4] Harrison RM, Yin J. Particulate matter in the atmosphere: Which particle properties are important for its effects on health? *Sci Total Environ* 2000, **249**: 85–101.

[5] Seaton A, Godden D, MacNee W, *et al*. Particulate air pollution and acute health effects. *Lancet* 1995, **345**: 176–178.

[6] Environmental Protection Agency. Nitrogen oxides (NO_x)—Why and how they are controlled. Technical Bulletin EPA 456/F-99-006R, 1999. Available at https://www3.epa.gov/ttncatc1/dir1/fnoxdoc.pdf.

[7] Madaniyazi L, Nagashima T, Guo Y, *et al*. Projecting ozone-related mortality in East China. *Environ Int* 2016, **92–93**: 165–172.

[8] Bell ML, McDermott A, Zeger SL, *et al*. Ozone and short-term mortality in 95 US urban communities, 1987–2000. *JAMA* 2004, **292**: 2372–2378.

[9] Mohan B, Yang W, Chou SK. Fuel injection strategies for performance improvement and emissions reduction in compression ignition engines—A review. *Renew Sust Energ Rev* 2013, **28**: 664–676.

[10] Luján JM, Guardiola C, Pla B, *et al*. Considerations on the low-pressure exhaust gas recirculation system control in turbocharged diesel engines. *Int J Engine Res* 2014, **15**: 250–260.

[11] Huang L, Wang X, Yao S, *et al*. Cu–Mn bimetal ion-exchanged SAPO-34 as an active SCR catalyst for removal of NO_x from diesel engine exhausts. *Catal Commun* 2016, **81**: 54–57.

[12] McEwen J-S, Anggara T, Schneider WF, *et al*. Integrated *operando* X-ray absorption and DFT characterization of Cu–SSZ-13 exchange sites during the selective catalytic reduction of NO_x with NH_3. *Catal Today* 2012, **184**: 129–144.

[13] Kostoglou M, Konstandopoulos AG. Effect of soot layer microstructure on diesel particulate filter regeneration. *AIChE J* 2005, **51**: 2534–2546.

[14] Okada A. Automotive and industrial applications of structural ceramics in Japan. *J Eur Ceram Soc* 2008, **28**: 1097–1104.

[15] Mizutani T, Matsuhiro K, Yamamoto N. Advanced structural ceramics—From research to applications. *J Ceram Soc Jpn* 2006, **114**: 905–910.

[16] Kamp CJ, Folino P, Wang Y, *et al*. Ash accumulation and impact on sintered metal fiber diesel particulate filters. *SAE Int J Fuels Lubr* 2015, **8**: 487–493.

[17] Nakatani K, Hirota S, Takeshima S, *et al*. Simultaneous PM and NO_x reduction system for diesel engines. SAE Technical Paper 2002-01-0957, 2002. Available at https://doi.org/10.4271/2002-01-0957.

[18] Jayaseelan DD, Lee WE, Amutharani D, et al. *In situ* formation of silicon carbide nanofibers on cordierite substrates. *J Am Ceram Soc* 2007, **90**: 1603–1606.

[19] Allam S, Abom M. Acoustic modelling and testing of diesel particulate filters. *J Sound Vib* 2005, **288**: 255–273.

[20] Bensaid S, Marchisio DL, Russo N, *et al*. Experimental investigation of soot deposition in diesel particulate filters. *Catal Today* 2009, **147**: S295–S300.

[21] Yu M, Luss D, Balakotaiah V. Regeneration modes and peak temperatures in a diesel particulate filter. *Chem Eng J* 2013, **232**: 541–554.

[22] Shyam A, Lara-Curzio E, Pandey A, *et al*. The thermal expansion, elastic and fracture properties of porous cordierite at elevated temperatures. *J Am Ceram Soc* 2012, **95**: 1682–1691.

[23] Gordon T, Shyam A, Lara-Curzio E. The relationship

between microstructure and fracture toughness for fibrous materials for diesel particulate filters. *J Am Ceram Soc* 2010, **93**: 1120–1126.

[24] Shyam A, Lara-Curzio E, Watkins TR, *et al*. Mechanical characterization of diesel particulate filter substrates. *J Am Ceram Soc* 2008, **91**: 1995–2001.

[25] Suszuki H, Ota K, Saito H. Mechanical properties of alkoxy-derived cordierite ceramics. *J Mater Sci* 1988, **23**: 1534–1538.

[26] Pandey A, Shyam A, Watkins TR, *et al*. The uniaxial tensile response of porous and microcracked ceramic materials. *J Am Ceram Soc* 2014, **97**: 899–906.

[27] Chen K, Martirosyan KS, Luss D. Transient temperature rise during regeneration of diesel particulate filter. *Chem Eng J* 2011, **176–177**: 144–150.

[28] Sappok A, Costanzo V, Bromberg L, *et al*. Vibration-induced ash removal from diesel particulate filters. In Proceedings of the 2014 ASME Internal Combustion Engine Division Fall Technical Conference, Volume 1: Large Bore Engines; Fuels; Advanced Combustion; Emissions Control Systems, 2014, DOI: 10.1115/ICEF2014-5570.

[29] Goren R, Gocmez H, Ozgur C. Synthesis of cordierite powder from talc, diatomite and alumina. *Ceram Int* 2006, **32**: 407–409.

[30] Njoya D, Elimbi A, Fouejio D, *et al*. Effects of two mixtures of kaolin-talc-bauxite and firing temperatures on the characteristics of cordierite-based ceramics. *J Build Eng* 2016, **8**: 99–106.